arXiv:cond-mat/0301467v2 [cond-mat.mes-hall] 19 Mar 2003

Quantum effects in small-capacitance single Josephson junctions

Michio Watanabe*
Semiconductors Laboratory, RIKEN (The Institute of Physical and Chemical Research),
2-1 Hirosawa, Wako-shi, Saitama 351-0198, Japan

David B. Haviland†
Nanostructure Physics, The Royal Institute of Technology (KTH),
SCFAB, Roslagstullsbacken 21, 106 91 Stockholm, Sweden

(Dated: 2 August 2002)

We have measured the current-voltage (I-V) characteristics of small-capacitance single Josephson junctions at low temperatures ($T = 0.02 - 0.6$ K), where the strength of the coupling between the single junction and the electromagnetic environment was controlled with one-dimensional arrays of dc superconducting quantum interference devices (SQUIDs). The single-junction I-V curve is sensitive to the impedance of the environment, which can be tuned *in situ*. We have observed Coulomb blockade of Cooper-pair tunneling and even a region of negative differential resistance, when the zero-bias resistance R_0' of the SQUID arrays is much higher than the quantum resistance $R_K \equiv h/e^2 \approx 26$ kΩ. The negative differential resistance is evidence of the coherent single-Cooper-pair tunneling within the theory of current-biased single Josephson junctions. Based on this theory, we have calculated the I-V curves numerically in order to compare them with the experimental ones at $R_0' \gg R_K$. The numerical calculation agrees with the experiments qualitatively. We also discuss the R_0' dependence of the single-Josephson-junction I-V curve in terms of the superconductor-insulator transition driven by changing the coupling to the environment.

PACS numbers: 74.50.+r, 73.23.Hk, 73.40.Gk
Phys. Rev. B **67**, 094505 (2003).

I. INTRODUCTION

Small-capacitance superconducting tunnel junctions provide an ideal system for studying the interplay between quantum mechanically conjugate variables: the Josephson-phase difference across the junction and the charge on the junction electrode. Their behavior is influenced by dissipation, such as discrete tunneling of quasiparticles, coupling to an electromagnetic environment, etc. The simplest and the most fundamental example is the single junction. Current-voltage (I-V) characteristics of single junctions have been the subject of extensive theoretical investigations.[1,2] A small capacitance C gives a large charging energy $e^2/2C$, and thus the theory predicts that at low enough temperatures, a *superconducting* small-capacitance tunnel junction behaves like an *insulator* so long as the junction is isolated from the electromagnetic environment. Experimentally, however, the observation of this charging effect (Coulomb blockade) in a single junction is not straightforward, because the measurement leads attached to the single junction should have a high enough impedance to isolate the junction.[1] For this reason, thin-film resistors were employed for the leads, and Coulomb blockade was successfully observed in single Josephson junctions.[3] Tunnel-junction arrays were also tried for the leads, and an increase of differential resistance around $V = 0$ was reported.[4,5]

We use one-dimensional (1D) arrays of dc superconducting quantum interference devices (SQUIDs) for the leads.[6] The advantage of this SQUID configuration is that the effective impedance of an array can be varied *in situ* by applying an external magnetic field perpendicular to the SQUID loop. Thus, the zero-bias resistance of the SQUID arrays at low temperatures can be controlled over several orders of magnitude. This phenomenon has been extensively studied in terms of the superconductor-insulator (SI) transition.[7,8,9,10] The single junction in our samples, on the other hand, does not have a SQUID configuration, and therefore its parameters are practically independent of the external magnetic field. This enables us to study the *same* single junction in *different* environments. We show that the I-V curve of the single junction is indeed sensitive to the state of the environment. Furthermore, we can induce a transition to a Coulomb blockade of the single junction by increasing the zero-bias resistance R_0' of the SQUID arrays. When R_0' is much higher than the quantum resistances: $R_K \equiv h/e^2 \approx 26$ kΩ for quasiparticles and $R_Q \equiv h/(2e)^2 \approx 6.5$ kΩ for Cooper pairs, single-junction I-V curve has a region of negative differential resistance. The negative differential resistance is a result of coherent single-Cooper-pair tunneling from the viewpoint of the theory for current-biased single Josephson junctions whose electromagnetic environment has a sufficiently high impedance.[1,2]

In the context of the theory, we calculate the I-V curves numerically by following Ref. 11, and compare with the experimental ones at $R_0' \gg R_K$. The numerical results are in qualitative agreement with the experiments,[12] however, some quantitative discrepancies suggest that even at $R_0' \gg R_K$, the single-junction I-V curve would be influenced by the environment. According to the perturbation theory[13,14,15] that deals with the

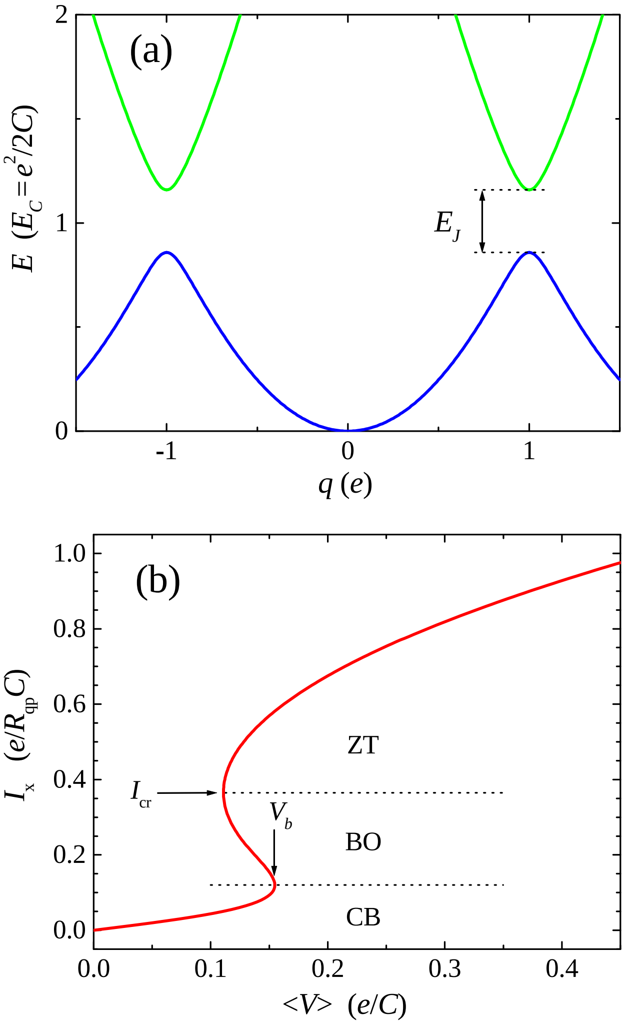

FIG. 1: (a) Energy diagram (energy eigenvalue in units of E_C vs. quasicharge) and (b) theoretical current-voltage characteristics for a single Josephson junction with $E_J/E_C = 0.3$ and $R_{\rm qp} = 10^2\,(h/\pi^2 e^2)$ at $k_BT/E_C = 0.3$, where E_J is the Josephson energy, $E_C \equiv e^2/2C$ is the charging energy, $R_{\rm qp}$ is the quasiparticle resistance, and k_BT is the thermal energy. (The energy diagram depends only on E_J/E_C.)

effect of a linear-impedance environment $Z(\omega)$ on single Josephson junctions, $\mathrm{Re}[Z(\omega)]$, or the dissipation, plays a key role. An insulating behavior characterized by the Coulomb blockade of Cooper-pair tunneling is expected for the single junction when $\mathrm{Re}[Z(\omega)] \gg R_Q$, i.e., the dissipation is sufficiently small, because the large $\mathrm{Re}[Z(\omega)]$ suppresses the charge fluctuation. The dissipative dynamics of single Josephson junctions has also been discussed by studying resistively shunted junctions both theoretically[2,16,17] and experimentally.[18,19] As the dissipation is increased (the shunt resistance is decreased), the tunneling of the Josephson phase is suppressed, and as a result the Josephson junction exhibits a transition from an insulator to a superconductor. The theoretical phase diagram[2] for this SI transition was supported by the experiments[18,19] qualitatively. The superconducting behavior has been observed experimentally in single Josephson junctions not only by shunting with a resistor but also by biasing with a low-impedance circuit,[20] i.e., by achieving a low-impedance electromagnetic environment. Thus, we expect that there should be a SI transition driven by the electromagnetic environment. We discuss the environment-driven SI transition in our system, where the environment is tunable with the SQUID arrays.

II. THEORY

The Hamiltonian of a single Josephson junction in an environment with sufficiently high impedance is written as

$$H = \frac{Q^2}{2C} - E_J \cos\phi\,, \tag{1}$$

where Q is the charge on the junction electrode, C is the capacitance of the junction, E_J is the Josephson energy, and ϕ is the Josephson-phase difference across the junction. The charge Q and $\hbar\phi/2e$ are quantum-mechanically conjugate valuables, and a set of the eigenfunctions are Bloch waves of the form

$$\psi(\phi) = u(\phi)\exp(i\phi q/2e)\,, \tag{2}$$

where q is called quasicharge and $u(\phi)$ is a periodic function,

$$u(\phi + 2\pi) = u(\phi)\,. \tag{3}$$

The energy eigenvalue E plotted as a function of q has a band structure, and in all the allowed bands, it is $2e$ periodic. An example of the energy diagram for $E_J/E_C = 0.3$, where $E_C \equiv e^2/2C$ is the charging energy, is shown in Fig. 1a. Under constant current bias $I_{\rm x}$, in the absence of quasiparticle or Cooper-pair tunneling, q increases uniformly in time according to

$$\frac{dq}{dt} = I_{\rm x}\,, \tag{4}$$

so that the state of the system advances toward higher q within a given band as time goes on. The average voltage is given by

$$\langle V\rangle = \sum_{i_b,q} P(i_b,q)\,\frac{dE(i_b,q)}{dq}\,, \tag{5}$$

where i_b is the band index and $P(i_b,q)$ is the probability that the system is in the state (i_b,q). The probability $P(i_b,q)$ can be calculated by solving a set of coupled differential equations of the form

$$\frac{dP(i_b,q)}{dt} = \sum_{i'_b,q'} A(i_b,q,i'_b,q')\,P(i'_b,q') = 0\,, \tag{6}$$

where the matrix element $A(i_b,q,i'_b,q')$ describes the rate of transition between the states (i_b,q) and (i'_b,q'). The dominant process for $A(i_b, q, i'_b, q')$ depends on the magnitude of $I_{\rm x}$.

An example of the theoretical *I*-*V* curve is shown in Fig. 1b. For sufficiently small $I_{\rm x}$ (region CB), the dominant process is stochastic quasiparticle tunneling, where q changes by e. This tunneling always occurs along the energy parabola $q^2/2C$, such that i_b changes by 0 or +1 if the initial state is in the lowest band ($i_b = 1$) and by ±1 for all the other initial states.[2] The rate for the quasiparticle tunneling is given by

$$\Gamma(\Delta E) = \frac{\Delta E/e^2 R_{\rm qp}}{\exp(\Delta E/k_B T) - 1} \ , \tag{7}$$

where $R_{\rm qp}$ is the quasiparticle resistance and ΔE is the difference in energy between the initial (i_b, q) and final (i'_b, q') states,

$$\Delta E \equiv E(i'_b, q') - E(i_b, q) \ . \tag{8}$$

At sufficiently low temperatures, the tunneling with $\Delta E > 0$ is extremely unfavorable, and the *I*-*V* curve is highly resistive (Coulomb blockade, region CB in Fig. 1b). For larger $I_{\rm x}$ (region BO in Fig. 1b), the quasicharge is frequently driven to the boundary of the Brillouin zone, $q = e$, then taken to $-e$ as a Cooper pair tunnels (Bloch oscillation). This process decreases $\langle V \rangle$, and as a result the *I*-*V* curve has a region of negative differential resistance, or "back bending," in the low-current part. For still larger $I_{\rm x}$ (region ZT in Fig. 1b), Zener tunneling becomes important, and $\langle V \rangle$ increases again. In Zener tunneling, no quasicharge is transferred but the state of the system jumps from one band to another as it passes by the gap between the bands. The probability of Zener tunneling from band i_b to $i_b + 1$ or vice versa is given by

$$P_Z = \exp\left[-\frac{\pi}{8} \frac{(\Delta E)^2}{i_b E_C} \frac{e}{\hbar I_{\rm x}} \right] \ . \tag{9}$$

Following Ref. 11 which takes into account the above tunneling processes (quasiparticle, Cooper pair, and Zener), we have calculated the *I*-*V* curve numerically.[27] The parameters for the calculation are E_J/E_C, k_BT/E_C, and

$$\alpha \equiv \frac{h}{\pi^2 e^2 R_{\rm qp}} \ . \tag{10}$$

The current and the voltage are in units of $e/R_{\rm qp}C$ and e/C, respectively.

As we have seen in Fig. 1b, a typical *I*-*V* curve consists of three regions, so that it is characterized by the local voltage maximum, or blockade voltage V_b, and the local current minimum, or crossover current $I_{\rm cr}$. (Here, we have to mention that the back-bending feature is blurred out if k_BT/E_C or α is increased considerably.) An analytical expression of V_b and $I_{\rm cr}$ has been obtained theoretically for limiting cases.[2] The value of V_b is a function of E_J/E_C, and given by

$$V_b \approx \begin{cases} 0.25\, e/C & \text{for } E_J/E_C \ll 1 \\ \delta_0/e & \text{for } E_J/E_C \gg 1, \end{cases} \tag{11}$$

as $T \to 0$, where

$$\delta_0 = \frac{e^2}{C}\, 8 \left(\frac{1}{2\pi^2}\right)^{1/4} \left(\frac{E_J}{E_C}\right)^{3/4} \exp\left[-\left(8\, \frac{E_J}{E_C}\right)^{1/2} \right] \tag{12}$$

is the half-width of the lowest energy-band. As for $I_{\rm cr}$,

$$I_{\rm cr} \sim \left(I_Z\ \frac{e}{R_{\rm qp} C} \right)^{1/2} \tag{13}$$

is expected for $\alpha \ll (E_J/E_C)^2 \ll 1$ and $T \to 0$, where

$$I_Z \equiv \frac{\pi}{8} \frac{e E_J^{\,2}}{\hbar E_C} \tag{14}$$

is the Zener breakdown current. Note that $I_{\rm cr}$ is much smaller than I_Z. When we compare our experimental results with the theory, we need theoretical prediction for finite k_BT/E_C, and arbitrary E_J/E_C and α. For this reason we have done the numerical calculation. The measured V_b and $I_{\rm cr}$ are compared with the calculation in Sec. IV C.

III. EXPERIMENT

A. Sample preparation and characterization

A schematic diagram of the Al/Al$_2$O$_3$/Al samples is shown in Fig. 2a. A single Josephson junction is at the center of Fig. 2a. The junction area is 0.1×0.1 μm^2. For a scanning electron micrograph of the single junction, see Fig. 1 of Ref. 6. On each side of the single junction, there are two leads enabling four-point measurements of the single junction. A part of each lead close to the single junction consists of a 1D array of dc SQUIDs. We show in Fig. 2b a scanning electron micrograph of a part of the SQUID array. Each of the electrodes in the array is connected to its neighbors by two junctions in parallel, thus forming a dc SQUID between nearest neighbors. The area of each junction in the SQUID array is 0.3×0.1 μm^2 and the effective area of the SQUID loop is 0.7×0.2 μm^2. All of the samples have the same configuration, except for the number N of junction pairs in each SQUID array. The samples are characterized by the normal-state resistance R_n of the single junction, the normal-state resistance r'_n per junction pair of the SQUID arrays, and N. The parameters of the samples are listed in Table I.

It is difficult to determine the uniformity of these 1D SQUID arrays when only the series resistance of all junctions can be measured. Previous work[8] showed that the variations of the normal-state resistance per junction pair were less than 6% for six arrays having nominally identical junctions made simultaneously on the same chip, with the number of junction pairs ranging from 7 to 255. Furthermore, critical-current switching at zero magnetic field for these arrays indicated a high degree of uniformity (Fig. 4 of Ref. 8), and the magnetic-field dependence of

TABLE I: List of the samples. R_n is the normal-state resistance of the single Josephson junction; E_J is the Josephson energy; $E_C \equiv e^2/2C$ is the charging energy, where the capacitance C is estimated from the junction area assuming 130 fF/μm^2; V_b and $I_{\rm cr}$ are the blockade voltage and the crossover current, respectively (see Figs. 1b and 6); $R_{\rm qp}$ is the quasiparticle resistance, which is estimated from the measured $I_{\rm cr}$ in Sec. IV C; N is the number of junction pairs in each SQUID-array lead; r'_n is the normal-state resistance per junction pair of the SQUID-array leads.

	Single Josephson junction					Leads	
Sample	R_n (kΩ)	E_J/E_C	V_b (μV)	$I_{\rm cr}$ (nA)	$R_{\rm qp}$ (kΩ)	N	r'_n (kΩ)
A	1.0	9	–	–	–	255	1.0
B	1.1	8	–	–	–	255	1.1
C	1.2	8	–	–	–	255	1.2
D	1.8	5	–	–	–	65	0.6
E	5.4	1.7	–	–	–	33	0.5
F	7.7	1.2	8	0.19	$(0.6-1.4)\times10^3$	255	1.0
G	9.0	1.0	10	0.19	$(0.5-1.2)\times10^3$	255	1.1
H	12	0.8	11	0.08	$(1-3)\times10^3$	33	1.2
I	17	0.5	25	0.08	$(1-3)\times10^3$	65	1.4
J	31	0.3	29	0.02	$(4-9)\times10^3$	65	1.9
K	41	0.21	28	0.02	$(4-9)\times10^3$	255	5
L	58	0.15	29	0.01	$(6-11)\times10^3$	255	7

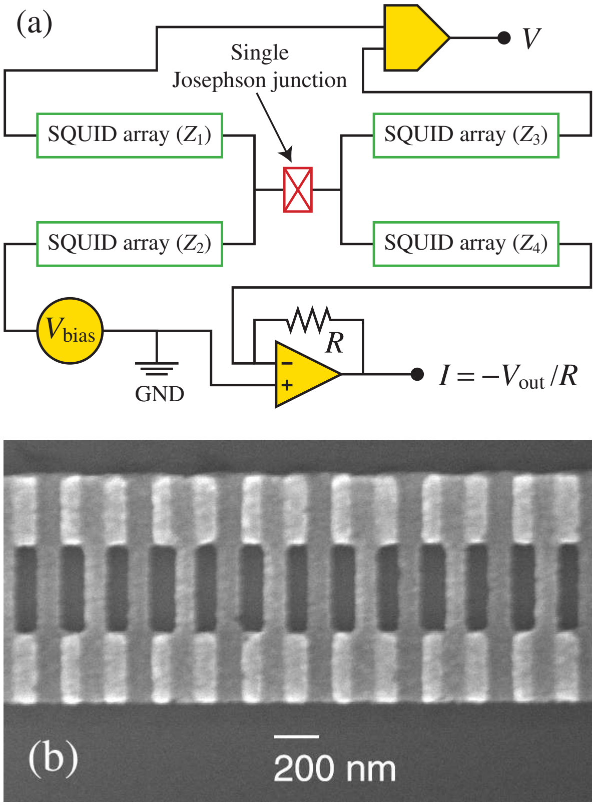

FIG. 2: (a) Schematic diagram of the samples and the circuit for measurements. (b) Scanning electron micrograph of a part of the 1D SQUID array.

the arrays was smooth. For the samples of this work, the uniformity of the SQUID arrays could be estimated by comparing the two arrays on the right- and left- hand sides of the single junction. On an average, the normal-state resistance of the arrays agreed to within 5%. However, if the tunnel-barrier thickness was identical for all junctions, one would expect $R_n/r'_n \approx 6$ from the junction area for our samples. In Table I, we see a large variation in $R_n/r'_n (= 1-17)$, which would be mainly due to the variation of R_n for the following reasons: In order to obtain r'_n, we do not examine one junction pair in the arrays, but measure two arrays in series and divide by $2N$. This kind of "averaging" does not occur when we determine R_n. Moreover, the single junction is much smaller than the junctions in the SQUID arrays, and small variations in the lithography and evaporation angle cause larger changes in the area of the smaller junction, thus leading to larger variations in the junction area and thereby the resistance and capacitance.

The tunnel junctions were fabricated on a SiO$_2$/Si substrate with electron-beam lithography and a double-angle shadow evaporation technique.[21] We employed a double-layer resist (ZEP520/PMGI) method in order to achieve a large enough undercut profile for the desired shift, which in our case was 0.2 μm. The electron-gun evaporation of Al was done at a rate of $0.1-0.4$ nm/s in a turbo-molecular-pumped vacuum system with the base pressure of $< 2\times10^{-6}$ Pa. The vacuum system is equipped with an angle stage, and with the stage tilted to an angle $+\theta \approx 13^\circ$, Al was deposited to a thickness of 20 nm. After deposition of the base electrode, O$_2$ was introduced into the chamber to a pressure of $1.3-4.0$ Pa for a period of $2-10$ min. The oxidation conditions, or the thickness of the Al$_2$O$_3$ layer, determines R_n and r'_n. After oxidation, the top layer of Al was deposited to a thickness of 30 nm with the stage tilted to an angle $-\theta$.

In the above process, bonding pads (0.3×0.35 mm^2) were also fabricated simultaneously, i.e., the pads are 20+30=50 nm-thick Al. Onto the pads, 25 μm-diameter Al wires were wedge bonded.

B. Measurements

The samples were measured in a ^{3}He-^{4}He dilution refrigerator (Oxford Instruments, Kelvinox AST-Minisorb) at $T = 0.02 - 0.6$ K. The temperature was determined by measuring the resistance of a ruthenium-oxide thermometer fixed at the mixing chamber. To measure the resistance of the thermometer, we used an ac resistance bridge (RV-Elekroniikka, AVS-47). Magnetic fields on the orders of $1 - 10$ mT were applied by means of a superconducting solenoid. In this magnetic-field range, the temperature error of ruthenium-oxide thermometers due to the magnetoresistance is negligibly small (e.g., a typical value of the error at $T = 0.05$ K is less than 0.1%).[22] The samples were placed inside a copper rf-tight box that was thermally connected to the mixing chamber. All the leads entering the rf-tight box were low-pass filtered by 1 m of Thermocoax cable.[23]

We measured the I-V curve of the single junction in a four-point configuration (see Fig. 2a). The bias was applied through one-pair of SQUID-array leads, and the potential difference was measured through the other pair of SQUID-array leads with a high-input-impedance instrumentation amplifier based on two operational amplifiers (Burr-Brown OPA111BM, $10^{13} - 10^{14}$ Ω input impedance according to the data sheet) and a preamplifier [Stanford Research Systems (SRS) SR560]. The current was measured with a current preamplifier (SRS SR570). When the voltage drop at the SQUID arrays was much larger than that at the single junction, the single junction was practically current biased.

The SQUID arrays could be measured in a two-point configuration (same current and voltage leads) on the same side of the single junction. Note that the two arrays are connected in series and that current does not flow through the single junction. In order to obtain R_n and r'_n, we measured at $T = 2 - 4$ K (above the superconducting transition temperature of Al).

IV. RESULTS AND DISCUSSION

A. SQUID arrays: tunable electromagnetic environment for the single junction

The effective Josephson energy E'_J between adjacent islands in the SQUID arrays is modulated periodically by applying an external magnetic field B perpendicular to the SQUID loop,

$$E'_J \propto \left| \cos \left(\pi \frac{BA}{\Phi_0} \right) \right| , \tag{15}$$

so long as B is sufficiently smaller than the critical field, where A is the effective area of the SQUID loop and $\Phi_0 = h/2e = 2 \times 10^{-15}$ Wb is the superconducting flux quantum. Figure 3 shows how the I-V curve of two SQUID arrays on the same side of the single junction changes depending on B. The I-V curve is Josephson-like at $B = 0$, while a Coulomb blockade is developed at $B = 7$ mT, where the normalized flux

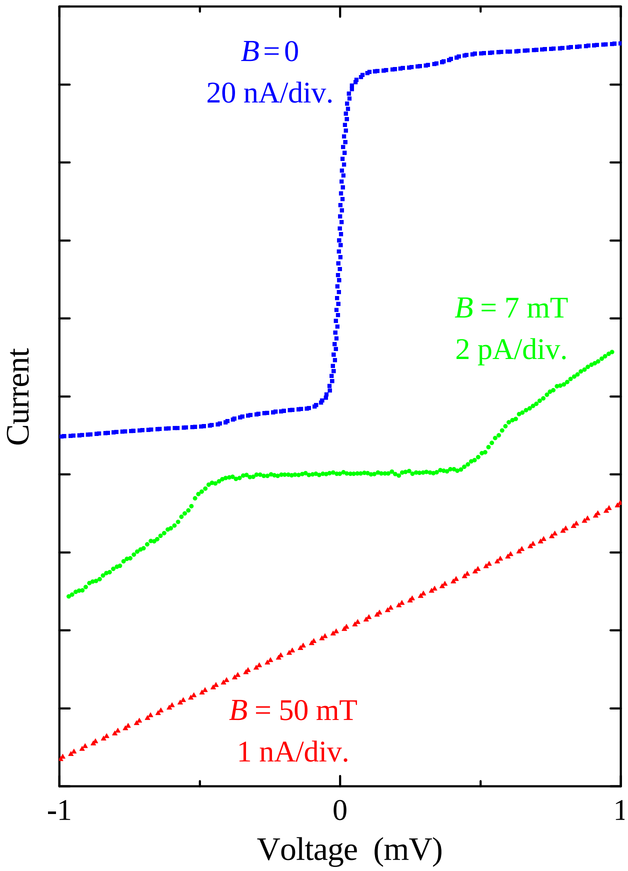

FIG. 3: Low-temperature ($T = 0.05$ K) current-voltage characteristics of two SQUID-array leads connected in series at three magnetic fields for Sample C. The origin of the current axis is offset for each curve for clarity. Note the difference in the current scale.

$$f \equiv \frac{BA}{\Phi_0} \tag{16}$$

is close to 1/2 for our samples with $A = 0.14$ μm^2. Note that the current scale for $B = 0$ is 10^4 times larger than that for $B = 7$ mT. In this manner, the I-V curve is varied periodically until B becomes comparable to the critical field. At $B = 50$ mT, the superconductivity is suppressed considerably, and the I-V curve is almost linear. The magnetic-field dependence of the SQUID arrays is summarized in Fig. 4, where the zero-bias resistance R'_0 of the same SQUID arrays is plotted vs. B. As expected from Eq. (15), R'_0 oscillates in the low-field regime. In the shaded regions, a Coulomb blockade is clearly observed and the maximum value of R'_0 can be as high as $10^9 - 10^{10}$ Ω (see Fig. 2 of Ref. 6 for R'_0 of Sample B at $0 \leq B \leq 9$ mT). At $B > 40$ mT, the oscillation is suppressed and R'_0 approaches the value in the normal state, $2Nr'_n$.

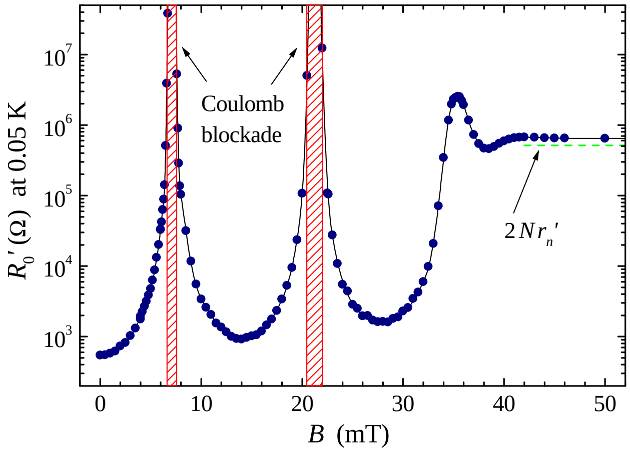

FIG. 4: Zero-bias resistance of the same SQUID-array leads as in Fig. 3 vs. external magnetic field at $T = 0.05$ K. The solid curve is a guide to the eye. The shaded boxes and the broken horizontal line represent the region where Coulomb blockade was clearly seen in the current-voltage curve and the normal-state resistance of the two leads, $2Nr_n'$, respectively.

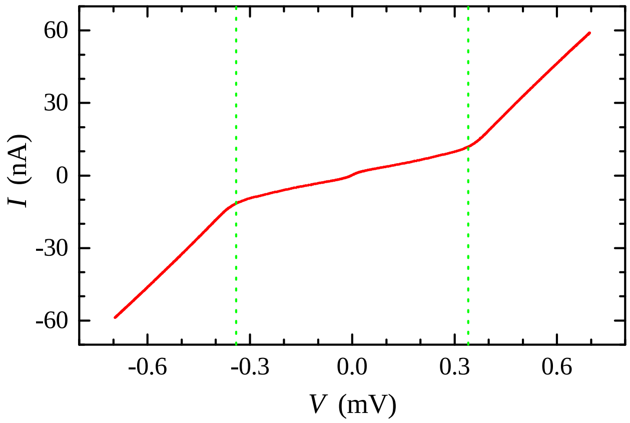

FIG. 5: Current-voltage characteristics of the single Josephson junction at $T = 0.04$ K and $f = 0$ for Sample G. For the definition of f, see Eq. (16) The vertical broken lines represent the superconducting-gap voltage $\pm 2\Delta_0/e$.

In summary of this subsection, the SQUID arrays, which act as an electromagnetic environment for the single junction in this work, can be tuned over a wide range *in situ* with f. Henceforth, we use f defined by Eq. (16) rather than B for the purpose of indicating the external field.

B. Coulomb blockade induced in the single Josephson junction by tuning the environment

In this subsection, we take Sample G for example. We look at the I-V curve and the influence of the electromagnetic environment on it. (The I-V curves of Sample I are shown in Figs. 3–5 of Ref. 6.) Figure 5 shows the I-V curves for the single junction at $f = 0$. The vertical broken lines represent the superconducting-gap voltage $\pm 2\Delta_0/e$, which is ± 0.34 mV for Al according to Ref. 24. In a conventional Josephson junction ($E_J \gg E_C$), a finite current flows at $V = 0$ as expected within the RCSJ (resistively and capacitively shunted junction) model.[25] This supercurrent has also been observed in small-capacitance Josephson junctions ($E_J \sim E_C$), and when a small-capacitance junction was biased with a carefully filtered low-impedance circuit,[20] the magnitude of the supercurrent reached the value predicted by the theory. Our single Josephson junction is biased with SQUID arrays, whose R_0' is much higher than the impedance (~ 24 Ω) of the biasing circuit of Ref. 20 even at $f = 0$. For the case of Fig. 5 (Sample G at $f = 0$), $R_0' = 0.21$ kΩ. Ingold and Grabert[15] considered how phase fluctuations suppress the supercurrent in a small-capacitance Josephson junction. The small capacitance of a junction is a source of phase fluctuations because the charge on the capacitance is the conjugate variable to the Josephson-phase difference. In addition, there is a strong relationship between the fluctuations and the electromagnetic environment. They assumed a purely Ohmic environment R, and showed that the supercurrent is rounded as R is increased. In such a context, the shape of the I-V curve in Fig. 5 may be explained for the region in the vicinity of $V = 0$, although our SQUID arrays are not represented by a purely Ohmic impedance. At higher voltages, finite currents still flow in Fig. 5 even within the superconducting gap. Theoretically, at a finite voltage $|V| < 2\Delta_0/e$, current can flow when the tunneling Cooper pairs can release their excess energy $2eV$, e.g., to the degrees of freedom in the electromagnetic environment. Quasiparticle excitations would also be responsible for the current especially at $|V| \sim 2\Delta_0/e$. Below we will concentrate on the immediate vicinity of $V = 0$ (typically ± 30 μV), where the I-V curve is most sensitive to the state of the electromagnetic environment.

Figure 6 shows how the single-junction I-V curve depends on the environment. As f is varied, the curve develops a Coulomb blockade. As we have mentioned in Sec. I, the Josephson energy of the single junction is independent of f because it does not have a SQUID configuration and the field $f\Phi_0/A < 7$ mT applied here is much smaller than the critical field. The electromagnetic environment for the single junction (the SQUID arrays), however, is strongly varied with f. The behavior of the single junction demonstrated in Fig. 6 does not result from the magnetic-field influence on the single-junction I-V curve, but rather from an environmental effect on the single junction. This experiment demonstrates in a direct way that the single-junction I-V curve is indeed sensitive to the electromagnetic environment.

Figure 7 shows the I-V curves of the two SQUID-array leads connected in series at the same f as in Fig. 6. The I-V curves of the leads are nonlinear, and in general the SQUID array is not described by a liner impedance model.[8] However, the environment may be characterized by R_0'. From (a) to (d) in Fig. 7, $R_0' = 0.21$ kΩ,

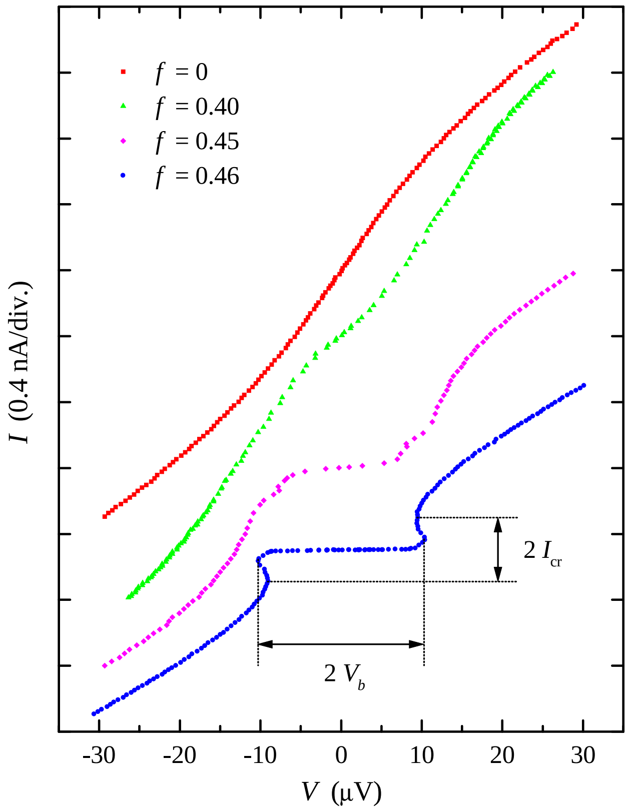

FIG. 6: Current-voltage (I-V) curves of the single Josephson junction in different environment at $T = 0.04$ K for Sample G. From top to bottom, the normalized flux defined by Eq. (16) is 0, 0.40, 0.45, and 0.46, respectively. The origin of the current axis is offset for each curve for clarity.

11 kΩ, 0.33 MΩ, and 6.5 MΩ, respectively. Coulomb blockade is distinct only when $R'_0 \gg R_K$, which is consistent with the theoretical conditions for the clear observation of Coulomb blockade in single junctions.[14] For an arbitrary linear environment characterized by $Z(\omega)$, $\mathrm{Re}[Z(\omega)] \gg R_K$ is required for the Coulomb blockade of single-electron tunneling and $\mathrm{Re}[Z(\omega)] \gg R_Q$ for that of Cooper-pair tunneling.[14] It is interesting to note that while the I-V curve of the leads is "Josephson-like" (differential resistance is lower around $V = 0$) at all f shown in Fig. 7, that of the single junction is "Coulomb-blockade-like" at $f = 0.40$ and exhibits a clear Coulomb blockade at $f \geq 0.45$.

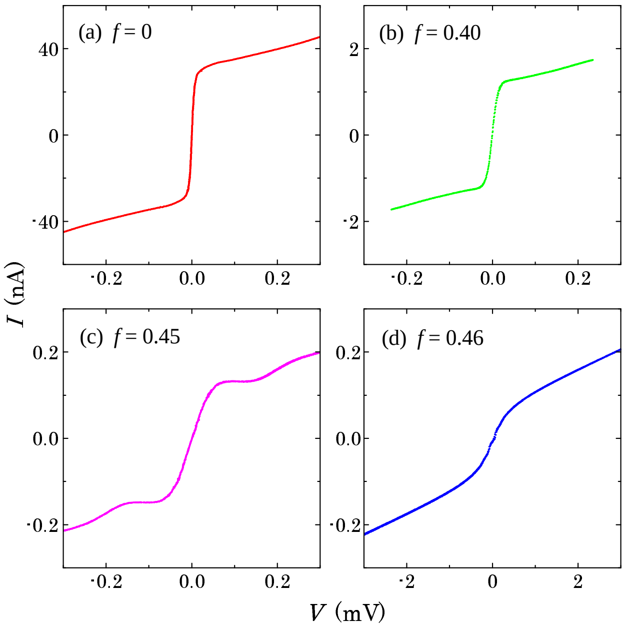

FIG. 7: Current-voltage curves of the two SQUID-array leads connected in series at $T = 0.04$ K for Sample G. From (a) to (d), the normalized flux defined by Eq. (16) is 0, 0.40, 0.45, and 0.46, respectively. Note the difference in the current scale, and that the voltage scale for (d) is 10 times larger than that for the others.

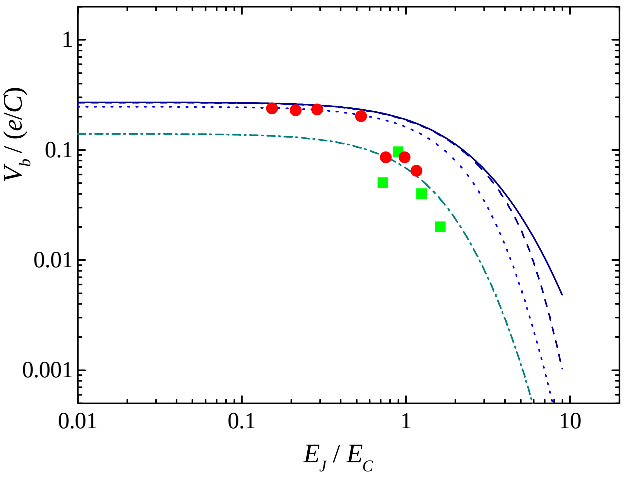

FIG. 8: Blockade voltage V_b divided by e/C as a function of E_J/E_C. From top to bottom, the curves represent the numerical calculations for normalized temperatures $k_BT/E_C = 0$, 0.02, 0.1, and 0.5, respectively. The boxes represent the samples with the nominal junction area of 0.01 μm^2 in Ref. 3.

C. Comparison with the numerical calculation

The region of negative differential resistance seen at the bottom curve of Fig. 6 is related to coherent tunneling of single Cooper pairs according to the theory[1,2] of a current-biased single Josephson junction in an environment with sufficiently high impedance. Following Ref. 11, we have calculated the blockade voltage V_b numerically as a function of E_J/E_C.[12] The numerical results are compared with the measured V_b in Fig. 8. The data from Ref. 3 for the samples with the same nominal junction area (0.1×0.1 μm^2) as in this work are also plotted. For Sample G we used the data at $f = 0.46$ (the bottom curve in Fig. 6) in order to obtain V_b. At $f = 0.46$ the voltage drop at the SQUID arrays is 10^2 times larger than that at the single junction, and the single junction is therefore considered to be current biased. Compare the voltage scale of Figs. 6 and 7d. We calculated E_J from R_n,

$$E_J = \frac{h\Delta_0}{8e^2 R_n} \ . \tag{17}$$

For E_C we employed $c_s = 130$ fF/μm^2, and with this value the experimental data, especially those for this work (the circles in Fig. 8), agree with the numerical calculation. Actually, a smaller value, $c_s = 45 \pm 5$ fF/μm^2 (Ref. 26), which was obtained for the junctions with 3×28 μm^2 and 7×54 μm^2, has been frequently employed.[3,5,7,8,9] Our apparently large c_s may be partly explained by distributed capacitance of the SQUID arrays or by the non-infinite impedance of the environment (SQUID arrays), which would have the effect of shunting the single junction with an additional capacitance (see Fig. 11). We also note that the uncertainty in c_s seems to be large when the junction area is on the order of 0.01 μm^2 or smaller, as we have discussed in Ref. 6.

Fixing $C = 1.3$ fF, we tried to reproduce the measured I-V curve by optimizing the other parameters of the numerical calculation, α and k_BT/E_C. Examples are shown in Fig. 9, where we adjusted α roughly by considering the current scale. For both Samples G and I, the slope of the experimental data at $|V| < V_b$ and $I \sim 0$ can be fit by adjusting α, so that it is consistent with the theoretical curve for $k_BT/E_C = 0.05$ ($T = 0.036$ K for $C = 1.3$ fF), which is close to the temperature of the mixing chamber, $0.02 - 0.04$ K. At higher bias currents, however, the theory predicts for $k_BT/E_C = 0.05$ a "back bending" much bigger than that in the experimental data. In terms of the magnitude of "back bending," the curves for higher temperatures, $k_BT/E_C = 0.3 - 0.6$ ($T = 0.21 - 0.43$ K), are more similar to the data. "Back bending" in the theoretical curve disappears when the temperature is raised to $k_BT/E_C = 0.8$ ($T = 0.57$ K). Although the theory explains the general shape of the measured I-V curve, it does not yield a complete agreement. It would be reasonable to assume that the effective temperature of the single junction depends on the bias current, and increases with increasing current due to heating. This assumption reduces the discrepancy between the experimental data and the theory. Another possible origin of the discrepancy would be the imperfect isolation of the single junction. While the theory assumes that the single junction is completely isolated from the environment, we have biased the single junction with the SQUID arrays having non-infinite R'_0. Moreover, the SQUID arrays are a nonlinear environment.

Finally in this subsection, we estimate $R_{\rm qp}$ from $I_{\rm cr}$ based on the theory. We plot the measured $I_{\rm cr}$ as a function of E_J/E_C in Fig. 10 together with some theoretical curves based on our numerical calculation. For the estimate of $R_{\rm qp}$ we used the numerical results for $k_BT/E_C = 0.3$ and 0.5 ($T = 0.21$ and 0.36 K), because with these values the numerical calculation gave an I-V curve similar to the experimental one around $I_{\rm cr}$ as we have seen in Fig. 9. The estimated $R_{\rm qp}$ is listed in Table I. The order of $R_{\rm qp}$ ($R_{\rm qp} = 10^0 - 10^1$ MΩ) and the ratio to R_n ($R_{\rm qp}/R_n = 10^2 - 10^3$) are within a reasonable range.

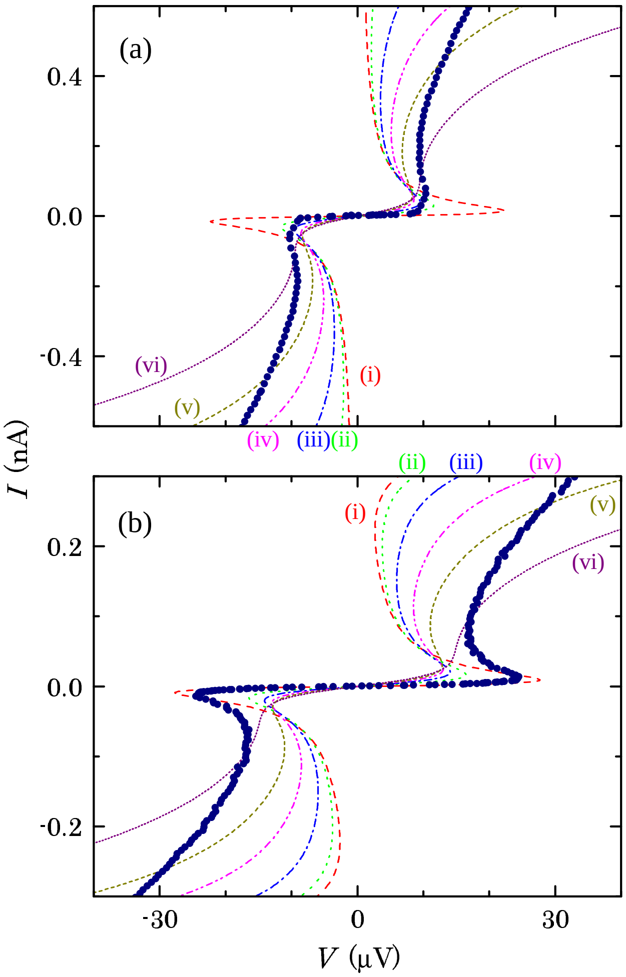

FIG. 9: Current-voltage curves of single Josephson junctions. (a) The measured curve (solid circles) of Sample G at $T = 0.04$ K and $f = 0.46$ is compared with the numerical calculations for $E_J/E_C = 0.53$ and $\alpha = 0.006$ [see Eqs. (10) and (16) for the definition of α and f, respectively]. (b) Sample I at $T = 0.02$ K and $f = 0.49$ with the calculatins for $E_J/E_C = 0.99$ and $\alpha = 0.003$. For both the figures, $C = 1.3$ fF is assumed in the calculations, and from (i) to (vi), $k_BT/E_C = 0.05$, 0.3, 0.4, 0.5, 0.6, and 0.8, respectively.

D. Superconductor-insulator transition in single Josephson junctions driven by the environment

The numerical calculation in the preceding subsection agrees with the experiment qualitatively, however, the apparently large c_s and the discrepancies in Fig. 9 suggest that the single junction would still be dependent on the environment even at $R'_0 \gg R_K$. The influence of a linear electromagnetic environment $Z(\omega)$ on small-

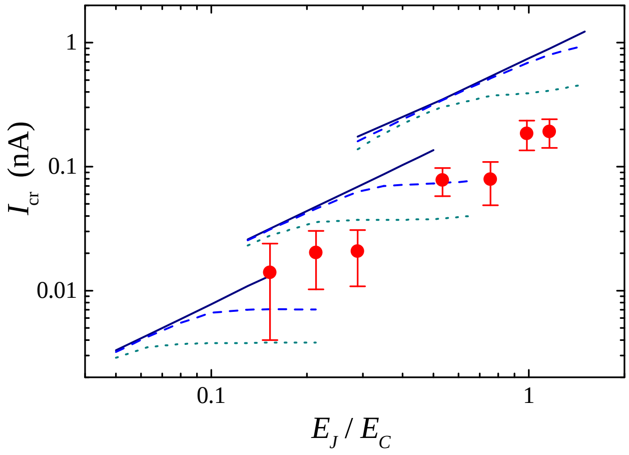

FIG. 10: Crossover current $I_{\rm cr}$ vs. E_J/E_C. The curves represent the numerical calculations for $C = 1.3$ fF, and from top to bottom $(\alpha,\ k_BT/E_C) = (10^{-2}, 0)$, $(10^{-2}, 0.3)$, $(10^{-2}, 0.5)$, $(10^{-3}, 0)$, $(10^{-3}, 0.3)$, $(10^{-3}, 0.5)$, $(10^{-4}, 0)$, $(10^{-4}, 0.3)$, and $(10^{-4}, 0.5)$, respectively. See Eq. (10) for the definition of α.

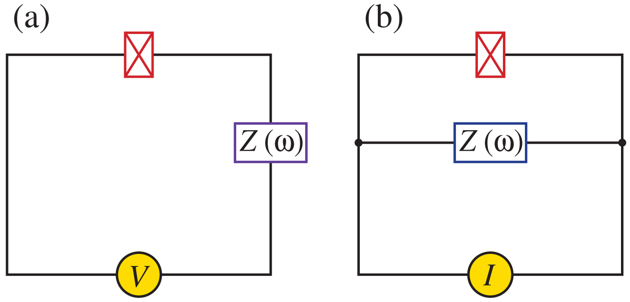

FIG. 11: (a) Small-capacitance single Josephson junction biased by an ideal voltage source with an electromagnetic environment $Z(\omega)$ in series. (b) An equivalent circuit to (a) when $I = V/Z(\omega)$, where the single junction is biased by an ideal current source and shunted by $Z(\omega)$.

capacitance Josephson junction has been studied in the framework of the perturbation theory[13,14,15] by modeling the whole circuit as in Fig. 11a. By assuming an Ohmic environment $Z(\omega) = R$, the Cooper-pair current-voltage characteristics have been calculated for $E_J/E_C \ll 1$. The theory predicts Coulomb blockade of Cooper-pair tunneling for $R_Q/R \ll 1$, and supercurrent at or in the vicinity $V = 0$ for $R_Q/R \gg 1$. By comparing Fig. 2a with Fig. 11a, we realize that the total impedance Z_t seen by the junction in Fig. 2a corresponds to Z in Fig. 11a. If we assume in Fig. 2a that the SQUID arrays alone determine the effective environment for the single Josephson junction at relevant frequencies, where all the four leads are shunted at the far ends of the SQUID arrays, and that the SQUID array is described by a linear impedance, we obtain $Z_t = \left(Z_1^{-1} + Z_2^{-1}\right)^{-1} + \left(Z_3^{-1} + Z_4^{-1}\right)^{-1} \approx Z_1$ (all the SQUID arrays are nominally the same). Note that the dc I-V curve is the result of high-frequency quasicharge dynamics of the single junction, and thus one must consider what the junction sees at high frequencies. The large capacitance introduced by the cryostat leads will effectively shunt the sample with a low impedance at the relevant frequencies. This is why we fabricated the SQUID arrays in the immediate vicinity of the single junction in order to avoid the lead capacitance shunting the single junction, and this is why we assume that the SQUID arrays alone determine the environment for the single junction. We have been characterizing the environment by the zero-bias resistance of two arrays measured in series, R_0'. Since $Z_t \approx Z_1$, it would be more appropriate to use $R_0'/2$. The factor of 2, however, is not very important in this work, and thus we keep using R_0'. We should note here that $Z \sim R_0'$ is a bold approximation. The I-V curves of the SQUID arrays are nonlinear as we have seen in Figs. 3 and 7, and in general the SQUID array is not described by a liner impedance. The frequency dependence[8] is also neglected in the approximation.

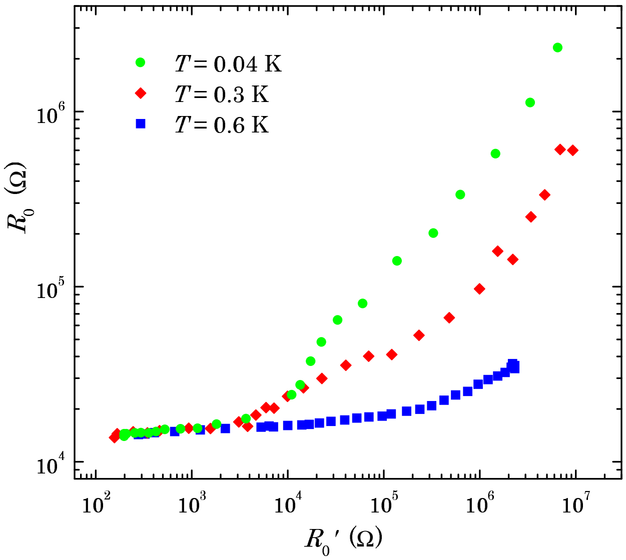

FIG. 12: Zero-bias resistance R_0 of the single Josephson junction vs. zero-bias resistance R_0' of the SQUID-array leads at $T = 0.04$, 0.3, and 0.6 K for Sample G.

In order to examine the R_0' dependence further, we plot in Fig. 12 the zero-bias resistance R_0 of the single junction vs. R_0' at three different temperatures for Sample G. At all the temperatures R_0 is a smooth function of R_0' and increases with increasing R_0', which supports the notion that the approximation $Z \sim R_0'$ is adequate. Even at the largest R_0', R_0 is still increasing with no sign of saturation. The top left point in Fig. 12 for $T = 0.04$ K and $R_0' = 6.5$ MΩ ($f = 0.46$) corresponds to the bottom I-V curve in Fig. 6. Thus, R_0 vs. R_0' also suggests that the single junction would still be influenced by the environment at $R_0' \gg R_K$. The change of R_0 is weak at $R_0' < 10^3 - 10^4$ Ω. This fact would be understood in the following context. In the limit of $R_0' \to 0$, the impedance of the electromagnetic environment for the Josephson junction at relevant frequencies is determined by the microwave impedance of the leads, which is usually of the order of the free-space impedance $Z_0 \approx 377\ \Omega$. Thus, when R_0' is of the order of Z_0 or smaller, our assumption that the SQUID arrays determine the environment is not valid, and $Z \sim Z_0$ irrespective of the value of R_0'. In Ref. 20, special care was taken in order to achieve $Z/Z_0 < 0.1$ at all relevant frequencies.

The interaction with a dissipative environment, or the dissipative dynamics of single Josephson junctions has also been studied theoretically[2,16,17] in the circuit shown in Fig. 11b with $Z(\omega) = R$. Note that the two circuits in Fig. 11 are equivalent when $I = V/Z(\omega)$. As the dissipation is increased, i.e., R is decreased, the Josephson junction undergoes a transition from an insulator to a superconductor. The phase diagram for this SI transition has been derived[2] and qualitatively supported by the experiments.[18,19] The phase ("superconductor" or "insulator") is usually determined by the I-V curve (or dV/dI vs. I curve[19]) at the lowest temperatures and/or the temperature dependence of the zero-bias resistance.[18] We also find evidence of the SI transition in the nonlinearity of the I-V curve. For Sample G, shown in Fig. 6, we see that the I-V curve is "Josephson-like" when the leads have $R_0' = 0.21$ kΩ ($f = 0$), whereas at $R_0' \geq 0.33$ MΩ ($f \geq 0.45$), there is a distinct Coulomb blockade. The temperature dependence of R_0 also supports the existence of the SI transition. We see in Fig. 12 that at $R_0' < 10^3 - 10^4\ \Omega$, R_0 has little temperature dependence, which is similar to the behavior of a 1D system[7,8,9] in the superconducting phase. At $R_0' > 10^4 - 10^5\ \Omega$, on the other hand, we see insulating behavior, where R_0 increases rapidly as the temperature is lowered.

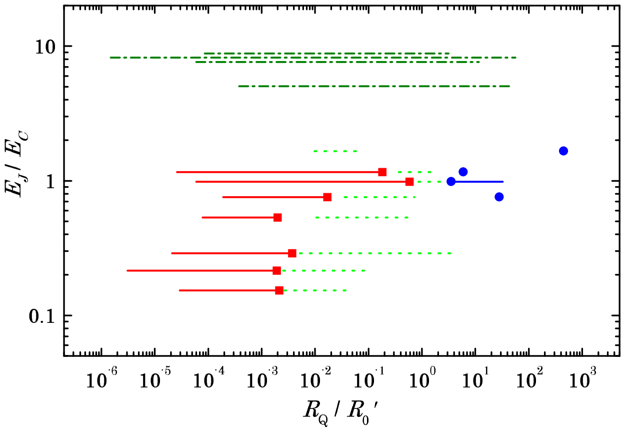

FIG. 13: Phase diagram for the superconductor-insulator transition in single Josephson junctions biased with tunable SQUID arrays. The transition is driven by the electromagnetic environment characterized by the zero-bias resistance R_0' of the SQUID arrays. The horizontal axis is the ratio of the quantum resistance $R_Q \equiv h/(2e)^2 \approx 6.5$ kΩ to R_0'. The vertical axis is the ratio of the Josephson energy E_J to the charging energy E_C in the single junction. See text for the meaning of the lines and symbols.

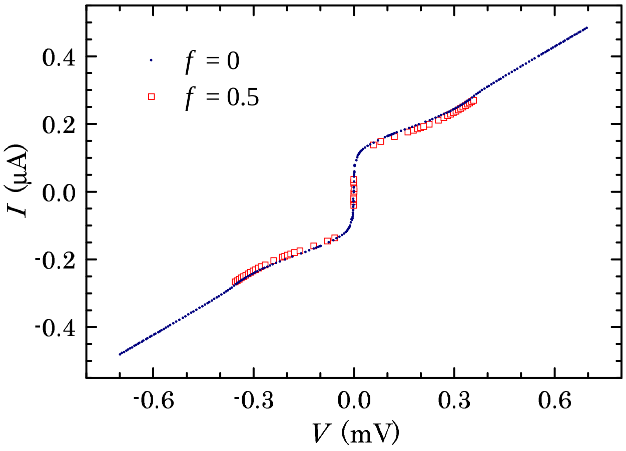

FIG. 14: Current-voltage characteristics of the single Josephson junction in two different environment ($f = 0$ and 0.5) at $T = 0.04$ K for Sample D. For the definition of f, see Eq. (16).

We show in Fig. 13 the phase diagram for the SI transition determined by the I-V curves at the lowest temperatures of all the samples studied in this work. Note that R_0' was varied over as large as nine orders of magnitude in this work. In Samples F–H, we observed the SI transition. The squares and the solid lines to the left of the squares indicate that insulating behavior (Coulomb blockade or "Coulomb-blockade-like" I-V curve) was observed. The circles and the solid lines to the right of the circles represent the superconducting phase ("Josephson-like" I-V curve). In the range denoted by broken lines, the I-V curve was almost linear, and it was hard to determine the phase. For Samples I–L (Sample E), the insulating (superconducting) phase alone was identified. Samples A–D have a large E_J/E_C (≥ 5), and we expect from Fig. 8 that their V_b is too small ($\ll 1\ \mu$V) to be detected in our dc measurements, i.e., the insulating phase is never identified. Indeed, the I-V curve of Samples A–D is almost independent of R_0'. As an example, we show in Fig. 14 the I-V curve of Sample D at $R_0' = 0.14$ kΩ ($f = 0$) and $R_0' = 2$ MΩ ($f = 0.5$). It is Josephson-like and in a contrast with the curve in Fig. 5. We do not discuss the SI transition for Samples A–D, and just indicate the R_0' range covered in the measurements by dot-dashed lines in Fig. 13. According to the theory[2] of single Josephson junctions with an Ohmic shunt R, the phase boundary is located at $R_Q/R = 1$ irrespective of the ratio E_J/E_C when the quasiparticle tunneling is not important ($\alpha \ll 1$) and the transition is driven solely by R. In Samples F–L, $\alpha = 10^{-4} - 10^{-2} \ll 1$ from Table I. It is interesting to see that Fig. 13, the phase diagram for our system with *non-Ohmic* environment, is consistent with the theoretical phase diagram where an *Ohmic* shunt is assumed.

V. CONCLUSION

We have studied the current-voltage (I-V) characteristics of single Josephson junctions biased with a tunable electromagnetic environment composed of SQUID arrays. We have demonstrated that the single junction is indeed sensitive to the state of the environment, and a Coulomb blockade is induced in the single junction by increasing the zero-bias resistance R_0' of the SQUID arrays. When R_0' is much higher than the quantum resistance $R_K \equiv h/e^2 \approx 26$ kΩ, a region of negative differential resistance has also been observed in the I-V curve of the single junction. The negative differential resistance is evidence of coherent single-Cooper-pair tunneling according to the theory of current-biased single Josephson junctions. Based on the theory we have calculated the I-V curves numerically. The calculation has reproduced the measured I-V curves at $R_0' \gg R_K$ qualitatively. We have also discussed the superconductor-insulator (SI) transition in single Josephson junction driven by the environment. We have characterized the environment by R_0' and determined the phase diagram for the transition. This phase diagram is consistent with the theoretical one for the SI transition in single Josephson junctions driven by an Ohmic shunt alone.

Acknowledgments

We are grateful to R. L. Kautz for great help in the numerical calculation, and to T. Kato and F. W. J. Hekking for fruitful discussions. This work was supported by Swedish NFR, and Special Postdoctoral Researchers Program and President's Special Research Grant of RIKEN. M. W. would like to thank the Japan Society for the Promotion of Science (JSPS) and the Swedish Institute (SI) for financial support.

---

[*] michio@postman.riken.go.jp; `http://www.riken.go.jp/lab-www/semiconductors/michio/`

[†] haviland@nanophys.kth.se; `http://www.nanophys.kth.se/`

[1] D. V. Averin and K. K. Likharev, in *Mesoscopic Phenomena in Solids*, edited by B. L. Altshuler, P. A. Lee, and R. A. Webb (Elsevier Science Publishers B. V., Amsterdam, 1991), chap. 6.

[2] G. Schön and A. D. Zaikin, Phys. Reports **198**, 237 (1990).

[3] D. B. Haviland, L. S. Kuzmin, P. Delsing, K. K. Likharev, and T. Claeson, Z. Phys. B **85**, 339 (1991).

[4] L. J. Geerligs, Ph.D. thesis, Delft Univ. of Tech., the Netherlands (1990).

[5] Y. Shimazu, T. Yamagata, S. Ikehata, and S. Kobayashi, J. Phys. Soc. Jpn. **66**, 1409 (1997).

[6] M. Watanabe and D. B. Haviland, Phys. Rev. Lett. **86**, 5120 (2001).

[7] E. Chow, P. Delsing, and D. B. Haviland, Phys. Rev. Lett. **81**, 204 (1998).

[8] D. B. Haviland, K. Andersson, and P. Ågren, J. Low Temp. Phys. **118**, 733 (2000).

[9] D. B. Haviland, K. Andersson, P. Ågren, J. Johansson, V. Schöllmann, and M. Watanabe, Physica C **352**, 55 (2001).

[10] M. Watanabe and D. B. Haviland, J. Phys. Chem. Solids **63**, 1307 (2002).

[11] U. Geigenmüller and G. Schön, Physica B **152**, 186 (1988).

[12] M. Watanabe, D. B. Haviland, and R. L. Kautz, Supercond. Sci. Technol. **14**, 870 (2001).

[13] G. Falci, V. Bubanja, and G. Schön, Z. Phys. B **85**, 451 (1991).

[14] G.-L. Ingold and Y. V. Nazarov, in *Single Charge Tunneling*, edited by H. Grabert and M. H. Devoret (Plenum Press, New York, 1992), chap. 2.

[15] G.-L. Ingold and H. Grabert, Phys. Rev. Lett. **83**, 3721 (1999).

[16] T. Kato and M. Imada, J. Phys. Soc. Jpn. **69**, 203 (2000).

[17] S. G. Chung, Phys. Rev. B **66**, 012503 (2002).

[18] R. Yagi, S. Kobayashi, and Y. Ootuka, J. Phys. Soc. Jpn. **66**, 3722 (1997).

[19] J. S. Penttilä, P. J. Hakonen, E. B. Sonin, and M. A. Paalanen, J. Low Temp. Phys. **125**, 89 (2001).

[20] A. Steinbach, P. Joyez, A. Cottet, D. Esteve, M. H. Devoret, M. E. Huber, and J. M. Martinis, Phys. Rev. Lett. **87**, 137003 (2001).

[21] D. B. Haviland, S. H. M. Persson, P. Delsing, and C. D. Chen, J. Vac. Sci. Technol. A **14**, 1839 (1996).

[22] M. Watanabe, M. Morishita, and Y. Ootuka, Cryogenics **41**, 143 (2001).

[23] A. B. Zorin, Rev. Sci. Instrum. **66**, 4296 (1995).

[24] C. Kittel, *Introduction to Solid State Physics* (John Wiley & Sons, New York, 1996), p. 344, 7th ed.

[25] M. Tinkham, *Introduction to Superconductivity* (MacGraw-Hill, New York, 1996), chap. 6, 2nd ed.

[26] A. W. Lichtenberger, C. P. McClay, R. J. Mattauch, M. J. Feldman, S.-K. Pan, and A. R. Kerr, IEEE Trans. Magn. **25**, 1247 (1989).

[27] The numerical code was written by R. L. Kautz.